energies

MDPI

Article

Determination of the Concentration of Propionic Acid in an Aqueous Solution by POD-GP Model and Spectroscopy

Mariusz Adamski, Mirosław Czechlowski, Karol Durczak and Tomasz Garbowski *

Department of Biosystems Engineering, Poznan University of Life Sciences, Wojska Polskiego 50, 60-627 Poznan, Poland; mariusz.adamski@up.poznan.pl (M.A.); miroslaw.czechlowski@up.poznan.pl (M.C.); karol.durczak@up.poznan.pl (K.D.)

* Correspondence: tomasz.garbowski@up.poznan.pl

Abstract: Biorefining and biorefineries are the future of industry and energy. It is still a long way to complete its implementation, but small biorefineries focused mainly on the production of fuels and energy are more and more frequent in rural areas and large areas located near big cities in which, in addition to fuels and energy, various organic substances of high market value are also produced. In order to optimize biogas production and to control methane fermentation processes, fast and accurate identification of carboxylic acid concentrations, including propionic acid as a precursor to acetic acid, is needed. In this study, a process quality control method was developed to evaluate the propionic acid content of an aqueous solution from the fermentation mass. The proposed methodology is based on near infrared spectroscopy with multivariate analysis and stochastic metamodeling with a denoising procedure based on proper orthogonal decomposition (POD). The proposed methodology uses the Bayesian theory, which provides additional information on the magnitude of the correlation between state and control variables. The calibration model was, therefore, constructed by using Gaussian Processes (GP) to predict propionic acid content in the aqueous solution using an NIR-Vis spectrophotometer. The design of the calibration model was based on absorbance spectra and calculation data from selected wavelength ranges from 305 nm to 2210 nm. Measurement data were first denoised and truncated to build a fast and reliable metamodel for precise identification of the acid content of an aqueous solution at a concentration from 0 to 5.66%. The mean estimation error generated by the metamodel does not exceed 0.7%.

Keywords: biogas; renewable energy source; spectroscopy; proper orthogonal decomposition; Gaussian Processes; propionic acid

Citation: Adamski, M.; Czechlowski, M.; Durczak, K.; Garbowski, T. Determination of the Concentration of Propionic Acid in an Aqueous Solution by POD-GP Model and Spectroscopy. *Energies* **2021**, *14*, 8288. https://doi.org/10.3390/en14248288

Academic Editor: Dino Musmarra

Received: 16 November 2021
Accepted: 7 December 2021
Published: 9 December 2021

1. Introduction

Research on biofuel production processes, including the fermentation process with the release of biogas, and research on oxygen stabilization processes indicate the important role of controlling the biomass conversion processes in relation to the broadly understood process efficiency [1,2]. The effective process of mineralization in anaerobic conditions is possible thanks to the protection of key technological parameters, including the chemical and biological properties of food substrates [3]. A good condition of a bacterial deposit depends, among others, on the control of parameters such as the following: temperature; pH; oxygen content; moisture content; intensity and quality of the mixing process; nutrient content; digestibility of polysaccharides contained in row fiber; carbon and nitrogen ratio; and the presence of key macronutrients [4,5]. The more difficult food digestibility is for bacterial deposits, the more important the process control issue is. In such cases, the inspection process should be intensified and streamlined [6,7]. The main element of the regulation and control mechanism of the methane fermentation process is to maintain the dynamics of the transformation of nutrients in key stages [8].

In the fermentation process with biogas production, the acidogenesis phase is distinguished during which the hydrolysis products produce carboxylic acids, which mainly

include valerian, formic and propionic acids [9]. Subsequently, compounds metabolized by bacteria (heterotrophy) in the process of acetogenesis cause the release of acetate [10]. The concentration of acetic acid in the process of oxygen stabilization and the level of acid buffering is an important control parameter with a predictive function in terms of auto-inhibition effects [9–12]. Thus, the level of propionic acid, thus, has a precursor function to the parameter of acetic acid concentration and the associated level of total inorganic carbon [7–13]. Thanks to the development of titration methods, it is possible to quantify the concentration of carboxylic acids expressed in the acetate's equivalent [8,14]. In addition to the methods dedicated to the detection of carboxylic acids (acetic acid and propionic acid) and based on chromatography, chemometric methods that use mathematical analysis of spectral spectra are also rapidly developing [15]. In this case, the advantages are consistent with titration methods but offer an extended possibility of qualitative and quantitative detection and logistical and economic improvements [16].

The post-fermentation or aerobic decomposition effluent contains characteristic fractions of products of chemical and biological transformations dissolved in moisture. These substances can be separated by classical methods and can be identified and quantified. Classical methods indicate that a liquid and clear filtrate can contain representative information for predicting propionic acid content in an aqueous solution [17–20]. Rapid detection of the precursor for the subsequent processes of acetogenesis and methanogenesis can be achieved by applying spectroscopic methods with the possibility of fast and precise response [21–29]. However, this requires prior construction and use of a reliable and fast metamodel for in situ testing.

Models for quick and precise estimation of the sought parameters (here, propionic acid concentration) are usually built on the basis of artificial neural networks or other soft computational methods. In the case of meta-models, all efforts to prepare and correlate them are transferred to the experimental and training phases. These models were tuned using a priori generated training pairs, namely measurements (input data) and targets (responses). The use of absorbance spectra as training data, especially over a wide wavelength range, involves a large amount of input data. Unfortunately, meta-models based on large amounts of noisy and often correlated data are not very effective. Therefore, input data should be first denoised and, if possible, also reduced to the smallest possible dimension. Reducing and denoising input measurement data can be performed, for example, by using methods based on principal component analysis (PCA).

The main idea of PCA is to reduce the multivariate dataset composed of a large number of correlated variables, while maintaining as much variation as possible in the dataset. In order to achieve the intended goal, a given set should be transformed into a new space of variables, called principal components (PC), which in the new system are no longer correlated. Additionally, they are ordered so that the first few components show the greatest variability present in all original variables. After determining all PCs, it is possible to reduce the dimensionality of the original variable space by selecting only the first few components, while maintaining a very high accuracy of approximation. In the literature, PCA is also known as singular value decomposition (SVD) or proper orthogonal decomposition (POD).

The original development (although still debatable) of proper orthogonal decomposition as a tool for graphical analysis was presented exactly 120 years ago by Pearson [30]. The method appears to have been independently developed over time in different research centers by different authors under different names. For example, Hotelling in the 1930s developed a method for processing statistical data and probability theory known as the Hotelling transformation [31]. A decade later, two scientists Karhunen [32] and Loeve [33] independently developed a theory of optimal expansions of continuous-time stochastic processes, now known as Karhunen–Loeve decomposition. Finally, Lumley [34] derived the idea of POD from independent investigations not only by Karhunen and Loeve but also in the mid-twentieth century by, e.g., Kosambi, Pougachev or Obukhov. The practical application of POD can be found, e.g., in [35–37].

Once experimental data are properly prepared by using PCA or POD, the only thing left to conduct is to select the appropriate metamodel. Ideally, finding a method that requires the smallest possible number of 'training samples' and at the same time is precise and robust is ideal. A surrogate based on Gaussian Processes (GP) meets both of the above-mentioned requirements [38–40]. It allows obtaining very precise results when the number of training examples is limited. In addition, GP allows obtaining not only an approximation of the average value of the solution sought but also its standard deviation, which allows for automatic and systematic improvements of the model. It is well known that a weak approximation of the model usually occurs where the values of the standard deviation are the highest [40,41]. Therefore, when the design of experiment is performed, it is easy to locate the space where it is necessarily too dense, and the experimental data can improve the solution.

The GP method used to prepare surrogate surfaces is usually formulated in the framework of Bayesian theory, which provides additional information on the magnitude of the correlation between state and control variables. Knowing the significance of the input–output correlation seems to be very important because on its basis it is possible to exclude from the model the parameters that do not affect measurable quantities [41]. Automatic reduction saves experimental efforts for finding parameters that turn out to be irrelevant in a given simulation. Such information can be obtained during the learning process and is similar to the results of a sensitivity analysis [42] often performed to validate the model.

However, GP-based stochastic surrogates have one significant drawback. Gaussian Processes are usually parameterized in terms of covariance functions, which means that the built models do not cope well with many outputs [39,41,43,44]. This problem, however, does not appear in the research problem analyzed in this article. Here, the only parameter is the concentration of propionic acid in the aqueous solution. The methodology presented in the paper, combining spectrometric analyses, stochastic modeling and noise reduction (with the reduction in dimensionality of the experimental data), is not only innovative but also allows estimating acid concentrations in an aqueous solution in situ with a maximum error of about 2%.

All the techniques described above, combined in one tool, make it possible to very accurately predict propionic acid concentrations in aqueous solution in the laboratory. When properly prepared and trained, the system is able to predict the correct response in a fraction of a second, provided the absorbance spectra are properly measured. To the best of our knowledge, there are no such implementations in laboratories that can estimate acid concentrations in aqueous solutions with such high accuracy.

2. Materials and Methods

2.1. Spectroscpy Setup

In this research study, pure propionic acid ($C_3H_6O_2$, catalog number 572940118) in the form of a transparent liquid with a density of 0.990 g cm^{-3} (20 °C) and pH = 2.5 (100 g L^{-1} H_2O, 20 °C) was used. The solvent used was distilled water (catalog number 524912001) with pH = 6.5, density of 1.00 g cm^{-3} and vapor pressure of 23 hPa (20 °C). The air temperature in the laboratory and temperature of the reagents were stabilized at 20 °C (Δ0.1 °C).

Vis-NIR absorbance spectra were obtained by transmission method using two fiber optic probes of the Tec5 AgroSpec spectrophotometer system, equipped with two detectors: MMS1 NIR enh. and PGS 2.2tc, both of which are from Carl Zeiss (Oberkochen, Germany). The RP-7 probe was used as a light source, which was located 25 mm above the sample in the optical axis of the receiving probe. The RP-7 probe generated a light beam that was to pass through the tested sample placed in a Petri dish made of borosilicate glass (see Figure 1). The A40 probe was 50 mm below the Petri dish with the sample and collected light transmitted through the sample. The Tec5 MultiSpec Pro 3.6 software was used to

record the spectra. Absorbance spectra were recorded in the wavelength range 305–2210 nm with an interpolated resolution of 5 nm.

(**a**) (**b**)

Figure 1. A sample of the training set; (**a**) a mixture of propionic acid and distilled water in a Petri dish; (**b**) a spectrophotometer with an RP-7 probe.

Each time, the acquisition of the spectrum of individual samples was repeated 20 times and averaged. Due to the intention to use the calibration model, a reference level of propionic acid concentrations in an aqueous solution was adopted. The concentration of carboxylic acids (including propionic acid) in wet methane fermentation processes is usually up to 5 g dm^{-3}.

Each sample was obtained by adding propionic acid to an initial volume of distilled water of 1000 cm^3. The dosing of propionic acid was determined in 1.0 cm^3 increments for sample concentrations of 0.1% to 5.66% (*v*/*v*). Each time the concentration after adding the next portion of propionic acid was recalculated by taking into account the changes in the total volume of the solution caused by previous additions. Finally, the proportion of propionic acid in the solution samples was presented as a percentage by mass concentration (% m/m).

After each increment, a sample of the aqueous propionic acid solution was mixed for 5 min and then placed in a petri dish with 30 cm^3 of the mixture, and absorbance spectra were recorded. The samples were homogenized using a hydraulic mixer. The selected method minimizes the access of solid, gaseous and chemical contaminants to the mixing chamber [45,46]. In total, sixty absorbance spectra, reflecting changes in the concentration of propionic acid in the aqueous solution from 0.1% to 5.66% (*v*/*v*), were recorded. Finally, the absorbance spectra for both pure propionic acid and pure aqueous solvent were also recorded. The samples were taken in accordance with EN ISO 8655.

In order to organize and support the search for optimal wavelength ranges from the point of view of, e.g., criterion of the applicability of the model for the recognition of propionic acid, a method consisting in comparing the absorbance spectra of pure propionic acid with the spectra of an aqueous solution and the characteristics of the standard deviation from the mean was used [47,48]. Models based on sets of absorbance spectra that have not been mathematically pretreated and with a baseline transformation applied are described in the next section.

2.2. Prper Orthogonal Decomposition

The sequence of direct measurements on the parameter $t_i (i = 1, \ldots, M)$ corresponding to a priori selected propionic acid concentration levels (in total 60; from 0.1% to 5.66% m/m) has been gathered by using an NIR-Vis spectrophotometer. All results are assembled in a matrix $\mathbf{U}_{N \times M}$ in which the m-th column $\mathbf{u}_m$ is a vector (snapshot) containing N experimental data (absorbance spectra in the wavelength range from 305 nm to 2210 nm) depending on the variable p_m (concentration of propionic acid in aqueous solution).

As the differences between the responses of the system results only from the variations of the sought parameters in the given range, the snapshots appear to be correlated, i.e., they form almost parallel vectors in their N-dimensional space ($N = 382$). In order to eliminate the correlation, the methods of truncation or compression of the information contained in the snapshot matrix $\mathbf{U} = [\mathbf{u}_1, \ldots \mathbf{u}_M]$ can be used by referring to POD. The computational procedures and mathematical theory related to POD have its origins far away in application fields and time, they have their origins distant in time and areas of application and they are currently used in the still up-to-date literature [49–53]. Only the specific procedure chosen and used for the present purpose is presented here, without examining analytical details.

The above defined matrix $\mathbf{U}$, preliminarily assembled from $M = 60$ laboratory tests, is used to construct the symmetric, positive (semi)definite matrix $\mathbf{D} = \mathbf{U}^T\mathbf{U}$. Its real and nonnegative eigenvalues λ_i and the corresponding eigenvectors $\mathbf{v}_i$ are then computed and used to generate the following orthonormal basis:

$$\mathbf{\Phi} = [\mathbf{\Phi}_1, \ldots, \mathbf{\Phi}_M], \tag{1}$$

with Equation (2).

$$\mathbf{\Phi}_i = \mathbf{U}\mathbf{v}_i\lambda_i^{-1/2}, \tag{2}$$

Due to orthonormality, matrix $\mathbf{A}_{M\times M}$, which collects the amplitudes $\mathbf{a}_M$ of the snapshots $\mathbf{u}_m$, is described by the following relationship:

$$\mathbf{A} = [\mathbf{a}_1, \ldots, \mathbf{a}_M] = \mathbf{\Phi}^T\mathbf{U}, \tag{3}$$

Thus, the following relationship is obtained.

$$\mathbf{U} = \mathbf{\Phi}\mathbf{A}, \tag{4}$$

The correlation between the snapshots (previously expected and noticed for the measured absorbance spectra in laboratory tests at different acid concentrations) means that many amplitudes $\mathbf{a}_i$ in the new basis $\mathbf{\Phi}$ can be ignored. A mathematical proof that eigenvalues λ_i quantify the negligibility of such amplitudes can be found in studies, e.g., [54]. Keeping only the $\overline{M}$ largest eigenvalues (say 2–4 from 60), with $\overline{M} \ll M$, the approximation $\overline{\mathbf{U}}_{N\times\overline{M}}$ of the snapshot matrix $\mathbf{U}_{N\times M}$ is obtained by using the truncated basis $\mathbf{\Omega}_{N\times\overline{M}}$ and the corresponding truncated amplitudes $\mathbf{X}_{N\times\overline{M}}$:

$$\overline{\mathbf{U}} = \mathbf{\Omega}\mathbf{X} \cong \mathbf{U}, \tag{5}$$

whence the following is obtained from.

$$\mathbf{X} = \mathbf{\Omega}^T\overline{\mathbf{U}}, \tag{6}$$

This procedure often proves to be computationally difficult and time consuming, but it only needs to be performed once for all as preparatory work to generate matrices $\mathbf{\Omega}$ and $\mathbf{X}$, which can be used, for example, on a small tablet to work in situ in the laboratory. From then on, the snapshot $\mathbf{u}^*$ corresponding to any new parameter vector t^* (new because not included in the training process) can now be evaluated through (pod6) by its truncated amplitude $\overline{M}$-vector $\mathbf{x}(t^*)$.

2.3. Gauusian Processes

In order to correctly describe the construction of the surrogate surface based on Gaussian Processes, the first thing is to consider is a Linear Regression (LR) model. In general, LR is a linear function of model parameters $\mathbf{w}$ and at the same time is a nonlinear

function of the input vector (i.e., truncated amplitude vector **x**), and it is usually defined as follows:

$$y(\mathbf{x}, \mathbf{w}) = \sum_{j=1}^{M} w_j \varphi_j(\mathbf{x}), \tag{7}$$

which is a linear combination of nonlinear and fixed basis functions $\varphi_j(\mathbf{x})$ of the input variables (e.g., polynomial or radial basis functions).

For the N given training patterns $(\mathbf{x}_n,\ t_n)$, $\mathbf{x}_n$ being the input vector and t_n the response for $n = 1 \ldots N$, the parameters **w** of the linear model can be solved by, for example, the penalized least squares method:

$$\mathbf{w} = \left(\mathbf{\Theta}^T \mathbf{\Theta} + \alpha \mathbf{I}\right)^{-1} \mathbf{\Theta}^T \mathbf{t}, \tag{8}$$

where $\mathbf{\Theta}_{\mathrm{N} \times M}$ is a design matrix with elements defined as $\theta_m(\mathbf{x}_n)$. The regularization parameter α is called a hyperparameter and can be obtained by using a validation set (similar to multilayer perceptrons) or by maximizing evidence of dataset $p(\mathbf{t}|\alpha)$ with respect to α [41] within Bayesian inference.

Reformulating the linear model in terms of dual representation allows obtaining the Gaussian process model. The training process of the linear model is performed here by minimizing a regularized error (i.e., $N \times N$ symmetric Gram matrix):

$$\mathbf{K} = \mathbf{\Theta}\mathbf{\Theta}^{\mathrm{T}} = \theta(\mathbf{x})^T \theta(\mathbf{x}') = k(\mathbf{x}, \mathbf{x}'), \tag{9}$$

where $k(\mathbf{x},\ \mathbf{x}')$ is a kernel function. The vector $\mathbf{k}_n = k(\bar{\mathbf{a}}_n,\ \mathbf{a})$ represents n-th row or column of **K** matrix.

The prediction for a new input $\mathbf{x}^*$ can be computed by the following formula:

$$GP(\mathbf{x}^*|\mathbf{x}, \mathbf{t}, \alpha) = k(\mathbf{x}, \mathbf{x}^*)^T (\mathbf{K} + \alpha \mathbf{I})^{-1} \mathbf{t} \tag{10}$$

where $\mathbf{t} = (t_1 \ldots t_N)^T$ is a vector of training target values, while $k(\mathbf{x},\ \mathbf{x}^*)$ is a covariance between the all other inputs and a new input $\mathbf{x}^*$.

Sine, according to Bayesian theory, is the dual representation of linear model resulting in the Gaussian process, and the kernel function is interpreted as a function of GP covariance. By using a regression model, it is possible to calculate the distribution of the target variable $y(\mathbf{x}^*)$ prediction for the new input vector $\mathbf{x}^*$. For Gaussian Processes, the conditional distribution $p(y|\mathbf{t})$ is the Gaussian distribution with mean determined by the following formula.

$$\mathrm{mean}(\mathbf{x}^*) = \mathbf{k}^T \mathbf{C}^{-1} \mathbf{t}, \tag{11}$$

Moreover, covariance is provided by the following:

$$\sigma^2(\mathbf{x}^*) = \mathbf{c} - \mathbf{k}^T \mathbf{C}^{-1} \mathbf{k}, \tag{12}$$

where $\mathbf{C}_{N \times M}$ is the covariance matrix provided by the following formula:

$$\mathbf{C}(\mathbf{x}, \mathbf{x}') = k(\mathbf{x}, \mathbf{x}') + \beta^{-1} \mathbf{I}, \tag{13}$$

where β is the variance of the target distribution and **I** is an identity matrix. The covariance matrix $\mathbf{C}(\mathbf{x},\ \mathbf{x}')$ defines a relationship in which the vectors **x** and $\mathbf{x}'$ closely adjacent in the input space generate highly correlated values of $y(\mathbf{x})$ and $y(\mathbf{x}')$ in the output space. A covariance function can be any function that will generate a specific non-negative covariance matrix for any ordered set of (input) vectors $(\mathbf{x}_1, \ldots, \mathbf{x}_N)$, e.g., a stationary, non-isotropic squared exponential covariance function $k(\mathbf{x}, \mathbf{x}')$ given by the following:

$$k(\mathbf{x}, \mathbf{x}') = \nu \exp\left(-\frac{1}{2} \sum_{i}^{M} \omega_i (x_i - x_i')^2\right) + b \tag{14}$$

where ν controls the vertical scale of the process, while b represents a bias that controls the vertical offset of the Gaussian process. The ω_i parameters control a different distance measure in each dimension. If ω_i is small then it has a little effect on the input and, therefore, the i-th input is downweighted. These hyperparameters play a very important role mainly because they possess a direct link to model sensitivities with respect to input parameters and thus provide a measure of the importance of input parameters.

After defining the covariance function, it is possible to make predictions of the new input vectors. Before that, however, it is necessary to determine the hyperparameters.

$$\mathbf{r} = [\nu, \omega_1, \ldots, \omega_M, b, \beta]. \tag{15}$$

In order to find those parameters, one can search for the most probable set by maximizing the log likelihood function given by the following:

$$\ln p(\mathbf{t}|\mathbf{r}) = \frac{1}{2}\ln|\mathbf{C}| - \frac{1}{2}\mathbf{t}\mathbf{C}^{-1}\mathbf{t} - \frac{N}{2}\ln 2\pi, \tag{16}$$

using any gradient-based optimization algorithms, such as a first-order batch Levenberg–Marquardt Algorithm (LMA) or Trust Region Algorithm (TRA) [55]. In this study, TRA, which provides fast convergence, was used.

2.4. Metamodel—Training and Testing

In order to properly train the model and then be able to reliably test it, first the experimental set was divided into training and testing data. A total of 10 vectors, spaced at equal intervals, were used for the test data, starting from the 6th record (0.588 m/m), every 6 to 60 (5.580 m/m), while the remaining 50 records were used for the model training.

In the first step, the absorbance spectrum in the full wavelength range from 305 nm to 2210 nm was used. The number of elements in truncated amplitude vectors varied from 5 to 30 in order to check for the value the best model performance can achieve. In the second step, the limited wavelength range was used according to preliminary observations.

A simple check of the exact truncation of the wavelength range was then carried out, where 9 combinations of the lower limit 1250, 1300 or 1350 and the upper limit 1750, 1800 or 1850 were used in the construction of POD. The check was performed with the amplitude vector reduced to a priori selected 3 elements. For further tests, the wavelength range was set at 1300–1800 nm.

It is expected that the fewer the elements in input vector **x**, the worse the estimate becomes, which is due to an insufficient amount of information carried by the truncated amplitude vectors. Similarly, if there are more elements, the estimation error becomes greater because the data contain more noise. Therefore, the search of an optimal level of truncation (from 2 to 8) in the narrowed wavelength range was also performed.

3. Results

Figure 2 shows all absorbance spectra of propionic acid concentration between 0 and 5.66% m/m in the full range of wavelengths (Figure 2a) and in the limited range (Figure 2b).

Figure 3 presents the absorbance spectra of the following: propionic acid, aqueous solution (average value for 60 samples with increasing concentration of propionic acid) and standard deviation from the average. Pure propionic acid has the highest absorbance in zone IV; therefore, it is expected that, also in this range, the absorbance graphs for all concentrations of aqueous propionic acid solutions should show the greatest sensitivity.

The preliminary results of model performance based on the full range of wavelengths of absorbance spectra are shown in Tables 1 and 2 and in Figure 4.

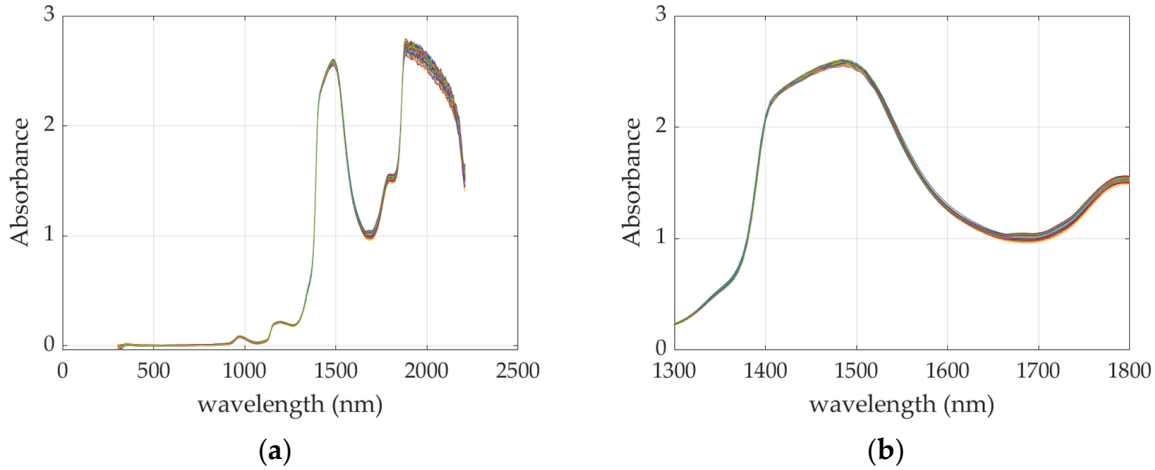

Figure 2. Absorbance spectra of propionic acid concentration between 0 and 5.66% m/m; (**a**) in the full range of wavelengths; (**b**) in the wavelength range limited to 1300–1800 nm.

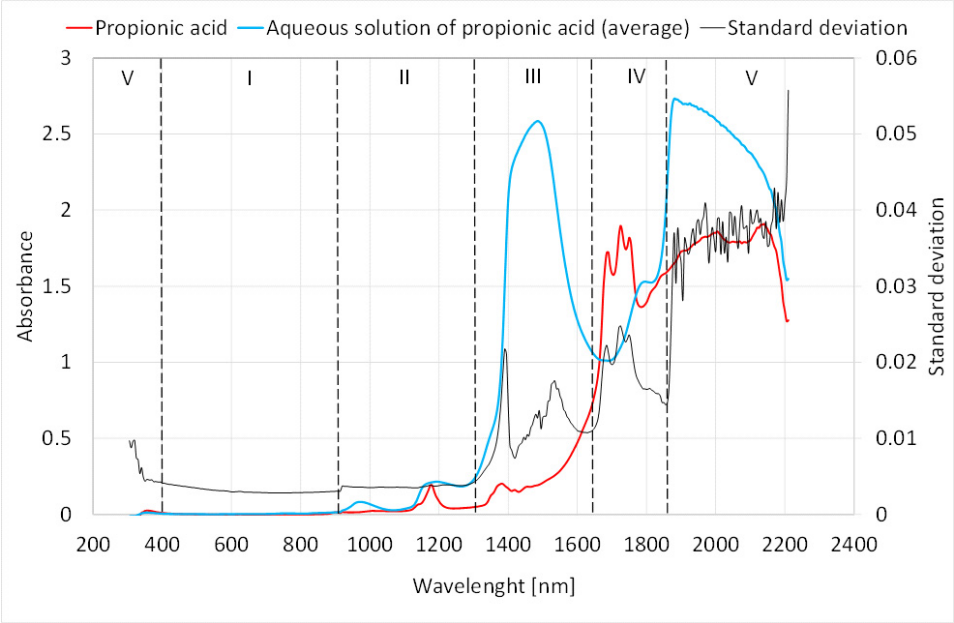

Figure 3. Absorption spectrum of pure propionic acid, averaged spectra of all analyzed levels of concentration of propionic acid in aqueous solution and standard deviation from the average with division of wavelength range into areas.

Table 1. Mean estimation error generated by a model trained by input data truncated to 5, 10, 15, 20, 25 and 30 amplitudes in the full range of wavelengths of absorbance spectra.

Number of Elements in the Truncated Amplitude Vector	Mean Estimation Error (%)
5	2.561
10	1.650
15	1.554
20	1.433
25	1.811
30	2.886

Table 2. Estimation error generated by a model trained by input data truncated to 5, 10, 15, 20, 25 and 30 amplitudes in the full range of wavelengths of absorbance spectra and for different concentration levels of propionic acid.

Propionic Acid Concentration	Estimation Error with Respect to Number of Elements in the Truncated Amplitude Vector (%)					
(% m/m)	30	25	20	15	10	5
0.58756	16.74	−5.978	0.877	−0.765	−0.217	−6.102
1.16825	1.031	−1.003	−1.813	−1.517	−1.850	−5.369
1.74220	−0.485	−1.462	2.648	1.988	2.149	1.275
2.30952	5.164	4.471	5.030	3.987	3.614	4.888
2.87033	0.447	1.731	−2.345	−1.747	−2.405	−0.736
3.42473	−0.820	0.891	−1.040	−0.133	0.478	0.601
3.97285	1.804	−0.116	0.253	−1.051	1.818	1.658
4.51477	−0.667	−1.122	0.052	−2.464	−0.404	−1.339
5.05061	1.070	1.224	0.223	−0.441	1.984	2.406
5.58048	0.635	0.111	0.046	1.441	1.579	1.236

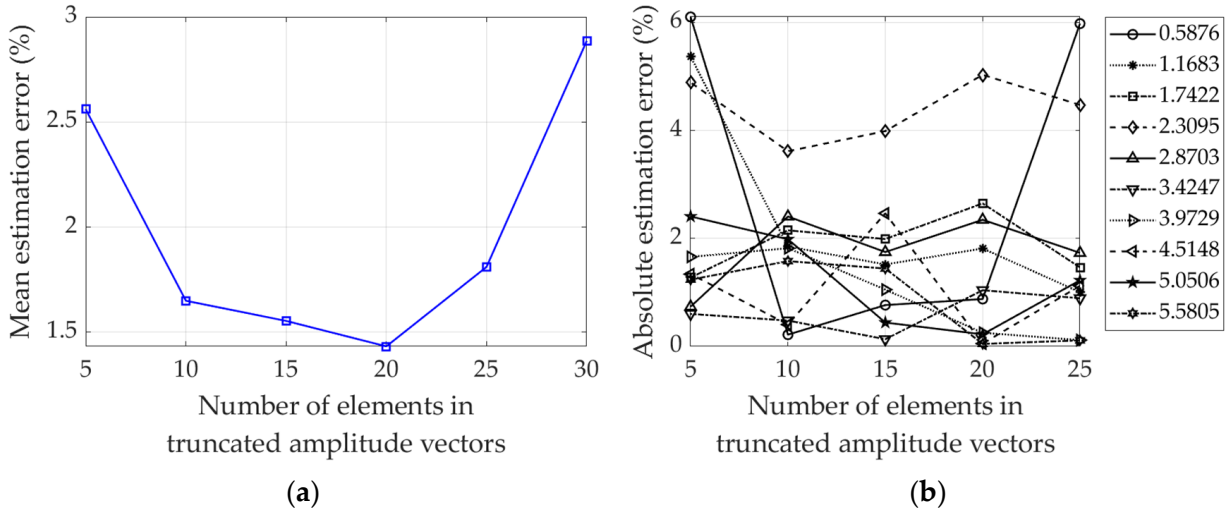

Figure 4. Estimation error generated by a model trained by input data truncated to 5, 10, 15, 20, 25 and 30 amplitudes in the full range of wavelengths of absorbance spectra; (**a**) mean estimation error; (**b**) absolute estimation error for different concentration levels of propionic acid.

Table 3 shows the normalized cumulative sum of all eigenvalues and the first eight eigenvalues calculated from matrix **D** of the model based on a truncated wavelength range to preliminary selected limits 1300–1800 nm.

Table 3. Normalized cumulative sum of all eigenvalues and the first eight eigenvalues computed from input data in the wavelength range truncated to 1300–1800 nm.

The Eigenvalue id	Eigenvalue	Normalized Cumulative Sum of Eigenvalues
1	10,271.4	99.99154
2	0.6824	99.99818
3	0.1666	99.99980
4	0.0039	99.99984
5	0.0028	99.99987
6	0.0021	99.99989
7	0.0018	99.99991
8	0.0015	99.99992

Table 4 shows the mean estimation error of the tuned model with truncated absorbance spectra at different ranges of the lower and upper wavelength limits.

Table 4. Mean estimation error generated by a model trained by input data truncated to 3 amplitudes at different bounds of wavelengths of absorbance spectra.

Min Wavelength (nm)	Max Wavelength (nm)	Mean Estimation Error (%)
1250	1750	0.923
1250	1800	0.709
1250	1850	0.833
1300	1750	0.997
1300	1800	0.677
1300	1850	0.804
1350	1750	1.047
1350	1800	0.719
1350	1850	0.819

The performance of a model tuned by input data truncated to different levels (from two to eight elements in the amplitude vector) are shown in Tables 5 and 6 as well as in Figure 5.

Table 5. Mean estimation error generated by a model trained by input data truncated to 2, 3, 4, 5, 6, 7 and 8 amplitudes in the wavelength range truncated to 1300–1800 nm.

Number of Elements in the Truncated Amplitude Vector	Mean Estimation Error (%)
2	13.44
3	0.677
4	0.668
5	0.682
6	0.681
7	0.898
8	1.047

Table 6. Estimation error generated by a model trained by input data truncated to 5, 10, 15, 20, 25 and 30 amplitudes in the wavelength range truncated to 1300–1800 nm and for different concentration levels of propionic acid.

Propionic Acid Concentration	Estimation Error with Respect to Number of Elements in the Truncated Amplitude Vector (%)						
(% m/m)	8	7	6	5	4	3	2
0.58756	1.776	0.850	−0.364	−0.392	−0.391	−0.059	−2.277
1.16825	3.462	3.022	2.193	2.196	2.154	2.240	33.12
1.74220	1.723	1.744	1.016	1.008	0.893	1.107	27.57
2.30952	−1.564	−1.609	−1.202	−1.207	−1.161	−1.102	−25.95
2.87033	−0.494	−0.558	−0.545	−0.543	−0.647	−0.555	−10.41
3.42473	0.086	0.021	0.148	0.144	0.137	0.234	14.05
3.97285	0.124	−0.047	−0.051	−0.047	−0.014	−0.074	−12.41
4.51477	0.289	0.247	0.318	0.314	0.323	0.403	−0.808
5.05061	0.822	0.877	0.810	0.813	0.789	0.753	−2.666
5.58048	−0.129	−0.003	−0.157	−0.156	−0.174	−0.237	5.125

The results obtained with a tuned model using a three-element amplitude vector and the wavelength range limited to 1300–1800 nm are presented in Table 7 and Figure 6.

It is clearly visible that in both models (Figure 6) the standard deviation is much higher for lower values of propionic acid concentrations. Furthermore, the normalized error is higher for acid concentrations below 2%, which indicates a greater level of noise in these concentration ranges.

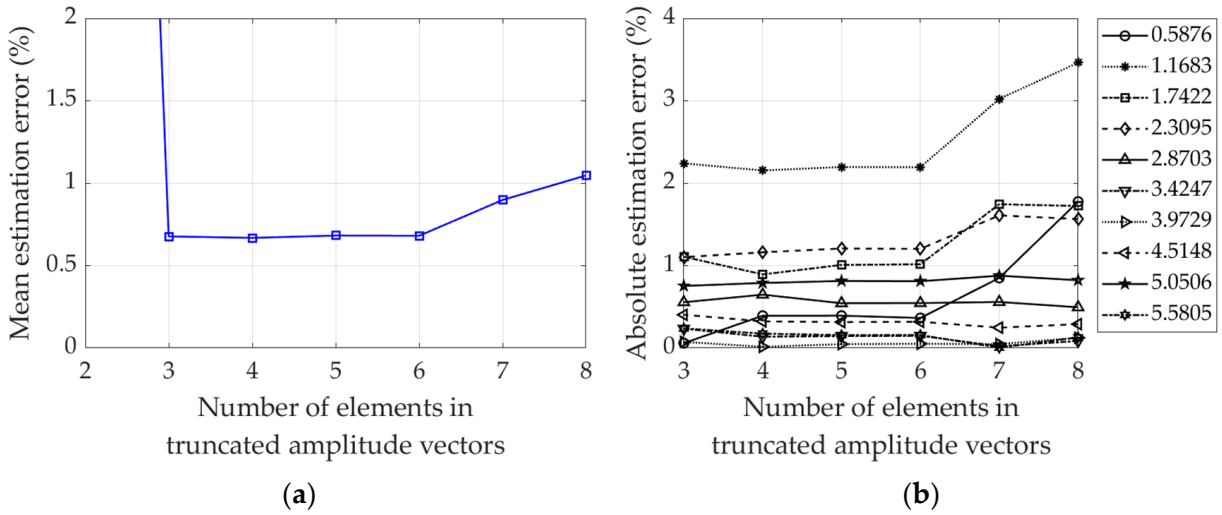

Figure 5. Estimation error generated by a model trained by input data truncated to 2, 3, 4, 5, 6, 7 and 8 amplitudes in the wavelength range truncated to 1300–1800 nm; (**a**) mean estimation error; (**b**) absolute estimation error for different concentration levels of propionic acid.

Table 7. The estimation (mean values, standard deviation and error) of a tuned model using a 3-element amplitude vector with a limited wavelength range (1300–1800 nm) of absorbance spectra.

Propionic Acid Concentration in Aqueous Solution		Estimation Error
Reference Value	Estimated Value	
(% m/m)	(% m/m)	(%)
0.58756	058755 ± 0.02497	0.001
1.16825	1.14166 ± 0.02136	2.276
1.74220	1.72256 ± 0.02650	1.127
2.30952	2.33508 ± 0.01488	−1.106
2.87033	2.88652 ± 0.01486	−0.564
3.42473	3.41694 ± 0.01622	0.227
3.97285	3.97585 ± 0.01821	−0.075
4.51477	4.49687 ± 0.01270	0.396
5.05061	5.01252 ± 0.01704	0.754
5.58048	5.59317 ± 0.02526	−0.227

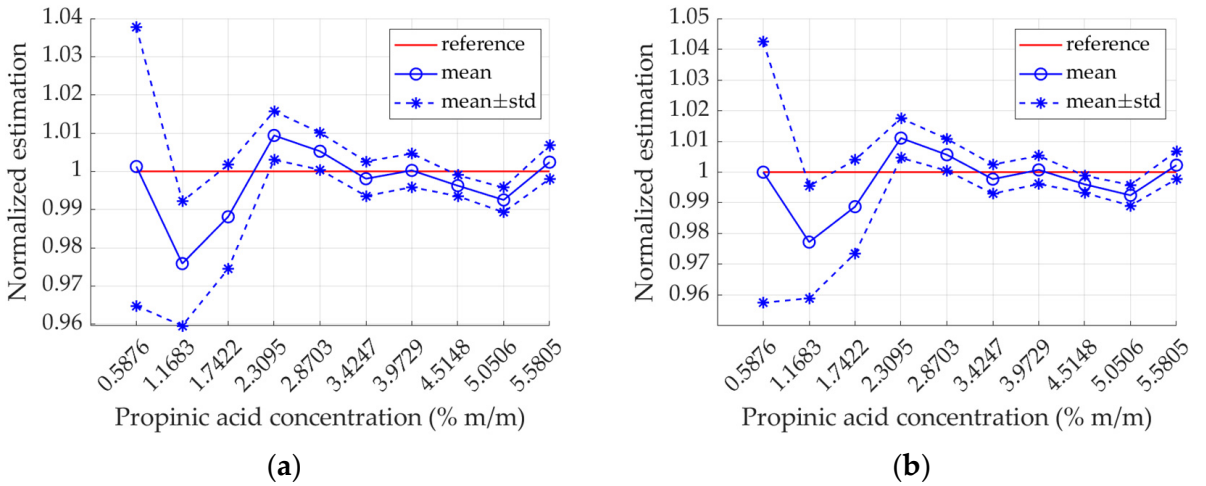

Figure 6. Normalized estimation of a tuned model using a 3-element amplitude vector with wavelength of absorbance spectra limited to (**a**) 920–1860 nm; (**b**) 1300–1800 nm.

4. Discussion

The composition of spectral information and standard deviation allows for the identification of characteristic areas:

- I (400–920 nm)—generally low absorption of radiation by propionic acid;
- II (920–1300 nm)—the maximum absorbance values for propionic acid and aqueous solution are similar;
- III (1300–1636 nm)—visible high absorbance for an aqueous solution; in the standard deviation, there is a visible change in absorbance caused by the absorbance peak for propionic acid just below 1400 nm;
- IV (1636–1860 nm)—visible high absorbance for propionic acid; standard deviation for the mean of the solution samples shows a very distinct absorbance variance caused by propionic acid;
- V (305–400 nm and 1860–2210 nm)—significant values of the standard deviation visible due to signal noise.

The obtained absorption spectrum of propionic acid contains an interesting wavelength range from 920 nm to 1860 nm, with peaks at 1150 nm, 1380 nm and between 1690 nm and 1780 nm and 1950 nm to 2170 nm. Propionic acid strongly absorbs radiation in the following wavelength range: 920-1300 nm and 1636–1860 nm in the near infrared range. The presence of water in the analyzed samples with solutions caused a significant differentiation of radiation absorption in the range from 1300 nm to 1636 nm and from 1790 nm to 1860 nm (see Figures 2 and 3).

Moreover, the greatest differences between the radiation adsorption by propionic acid and aqueous solution of propionic acid at a given acid concentration can be observed in range III and IV. Section II shows similar absorbance values for both propionic acid and aqueous solution of propionic acid.

It is clear from the analyses that the models that uses the full spectrum in the wavelength range from 305 to 2210 nm are burdened with greater errors, because the measurement data contain a large amount of noise located in the I and V regions (see Figure 2). This is evidenced by the results presented in Tables 1 and 2 and Figure 3. The largest mean estimation error, changing from 1.81% to 5.03%, is generated by the model for propionic acid concentration from 1% to 3% m/m. The best results are achieved when training data were truncated to 20 amplitudes.

The results generated by models trained with the absorbance spectrum in the indicated wavelength ranges are much better (see Tables 5–7 as well as Figures 5 and 6), and the learning process is much more stable. In this case, the problem of overfitting is much less common because only three amplitudes are used, which significantly reduces the amount of noise in the training data. The highest mean estimation error, ranging from 1.11% to 2.28%, is generated by the model for propionic acid concentrations from 1.15% to 2.30% m/m. Regardless of whether the analysis used the wavelength range only in the III and IV range or in the II–IV range, the average estimation error did not exceed 0.7%.

5. Conclusions

The results of this study confirm the possibility of using spectrometric measurements to monitor the content of propionic acid in aqueous solutions in an environment similar to methane fermentation. The obtained calibration models correspond to the assumptions of the accuracy of rapid detection methods in the quantitative analysis of volatile fatty acids, such as the Nordman DOC316.52.93087. The results of the research study indicated that further research is justified and should be focused on validation under the conditions of a quasi-continuous fermentation processes, which is an important step in improving prediction models.

The obtained results showed that propionic acid calibration models for which the wavelength ranges were determined using qualitative indicators are more effective than the models with non-selective detection ranges. On the basis of the research results, it is possible to undertake further studies aimed at building the measurement system. The

new measurement system, based on the proposed research method, renders it possible to evaluate the quality parameters of methane fermentation online at a laboratory scale. The proposed methodological solution also has implementation potentials, as this method corresponds to related identification and predictive solutions used for the production of biofuels [56]. This approach can easily be implemented in any laboratory equipped with a spectrometer, provided that the training process is carried out a priori. The method proposed here can also be extended to multi-component systems of aqueous solutions. All efforts to improve biogas production are very current and important trends in terms of energy consumption, production and estimates as well as their impact on emissions [57].

Author Contributions: Conceptualization, M.A., M.C., K.D. and T.G.; methodology, M.A., M.C., K.D. and T.G.; software, T.G.; validation, M.A., M.C. and T.G.; formal analysis, M.A. and T.G.; investigation, M.A., M.C. and T.G.; resources, M.A.; data curation, M.C.; writing—original draft preparation, M.A. and T.G.; writing—review and editing, M.A., K.D. and T.G.; visualization, M.A. and T.G.; supervision, K.D.; project administration, K.D. and T.G.; funding acquisition, M.C. and T.G. All authors have read and agreed to the published version of the manuscript.

Funding: The APC was funded by the Ministry of Science and Higher Education in Poland under the Regional Initiative Excellence programme 2019–2022, Project No. 005/RID/2018/19.

Institutional Review Board Statement: Not applicable.

Informed Consent Statement: Not applicable.

Data Availability Statement: The data presented in this study are available upon request from the corresponding author.

Acknowledgments: The publication was co-financed within the framework of Ministry of Science and Higher Education program as "Regional Initiative Excellence" in years 2019–2022, Project No. 005/RID/2018/19.

Conflicts of Interest: The authors declare no conflict of interest.

References

1. Wu, D.; Li, L.; Zhao, X.; Peng, Y.; Yang, P.; Peng, X. Anaerobic digestion: A review on process monitoring. *Renew. Sustain. Energy Rev.* **2019**, *103*, 1–12. [CrossRef]
2. Makan, A.; Fadili, A.; Oubenali, M. Interaction of physicochemical parameters during pressurized in-vessel composting of food waste. *Bioresour. Technol. Rep.* **2020**, *10*, 100350. [CrossRef]
3. Li, L.; He, Q.; Wei, Y.; He, Q.; Peng, X. Early warning indicators for monitoring the process failure of anaerobic digestion system of food waste. *Bioresour. Technol.* **2014**, *171*, 491–494. [CrossRef]
4. Li, D.; Chen, L.; Liu, X.; Mei, Z.; Ren, H.; Cao, Q.; Yan, Z. Instability mechanisms and early warning indicators for mesophilic anaerobic digestion of vegetable waste. *Bioresour. Technol.* **2017**, *245*, 90–97. [CrossRef]
5. Adamski, M.; Szaferski, W.; Gulewicz, P.; Majtkowski, W. Silage of Switchgrass (Panicum Virgatum) as a Bioenergy Feedstock in Poland. In *Practical Aspects of Chemical Engineering, Selected Contributions from PAIC 2017*; Lecture Notes on Multidisciplinary Industrial Engineering; Springer: Cham, Switzerland, 2018; pp. 1–15, ISBN 978-3-319-73978-6. [CrossRef]
6. Durczak, K.; Adamski, M.; Mitkowski, P.T.; Szaferski, W.; Gulewicz, P.; Majtkowski, W. Chemical Processing of Switchgrass (Panicum Virgatum) and Grass Mixtures in Terms of Biogas Yield in Poland. In *Practical Aspects of Chemical Engineering, Selected Contributions from PAIC 2017*; Lecture Notes on Multidisciplinary Industrial Engineering; Springer: Cham, Switzerland, 2018; pp. 85–99, ISBN 978-3-319-73978-6. [CrossRef]
7. Kandela, T.P.; Sutaryo, S.; Møller, H.B.; Jørgensen, U.; Lærke, P.E. Chemical composition and methane yield of reed canary grass as influenced by harvesting time and harvest frequency. *Bioresour. Technol.* **2013**, *130*, 659–666. [CrossRef] [PubMed]
8. Kandel, T.P.; Gislum, R.; Jørgensen, U.; Lærke, P.E. Prediction of biogas yield and its kinetics in reed canary grass using near infrared reflectance spectroscopy and chemometrics. *Bioresour. Technol.* **2013**, *146*, 282–287. [CrossRef]
9. Ahring, B.K.; Sandberg, M.; Angelidaki, I. Volatile fatty acids as indicators of process imbalance in anaerobic digesters. *Appl. Microbiol. Biotechnol.* **1995**, *43*, 559–565. [CrossRef]
10. Ghasimi, D.S.; Tao, Y.; de Kreuk, M.; Abbas, B.; Zandvoort, M.H.; van Lier, J.B. Digester performance and microbial community changes in thermophilic and mesophilic sequencing batch reactors fed with the fine sieved fraction of municipal sewage. *Water Res.* **2015**, *87*, 483–493. [CrossRef]
11. Gourdon, R.; Vermande, P. Effects of propionic acid concentration on anaerobic digestion of pig manure. *Biomass* **1987**, *13*, 1–12. [CrossRef]

12. Boe, K.; Batstone, D.J.; Steyer, J.P.; Angelidaki, I. State indicators for monitoring the anaerobic digestion proces. *Water Res.* **2010**, *44*, 5973–5980. [CrossRef]
13. Hansson, M.; Nordberg, A.; Sundh, I.; Mathisen, B. Early warning of disturbances in a laboratory-scale MSW biogas process. *Water Sci. Technol.* **2002**, *45*, 255–260. [CrossRef]
14. Charnier, C.; Latrille, E.; Jimenez, J.; Lemoine, M.; Boulet, J.C.; Miroux, J.; Steyer, J.P. Fast characterization of solid organic waste content with near infrared spectroscopy in anaerobic digestion. *Waste Manag.* **2017**, *59*, 140–148. [CrossRef]
15. Jacobi, H.F.; Moschner, C.R.; Hartung, E. Use of near infrared spectroscopy in monitoring of volatile fatty acids in anaerobic digestion. *Water Sci. Technol.* **2009**, *60*, 339–346. [CrossRef] [PubMed]
16. Hansson, M.; Nordberg, A.; Mathisen, B. On-line NIR monitoring during anaerobic treatment of municipal solid waste. *Water Sci. Technol.* **2003**, *48*, 9–13. [CrossRef] [PubMed]
17. Eryildiz, B.; Lukitawes; Taherzadeh, M.J. Effect of pH, substrate loading, oxygen, and methanogens inhibitors on volatile fatty acid (VFA) production from citrus waste by anaerobic digestion. *Bioresour. Technol.* **2020**, *302*, 122800. [CrossRef] [PubMed]
18. Montañés, R.; Pérez, M.; Solera, R. Mesophilic anaerobic co-digestion of sewage sludge and a lixiviation of sugar beet pulp: Optimisation of the semi-continuous proces. *Bioresour. Technol.* **2013**, *142*, 655–662. [CrossRef]
19. Li, D.; Ran, Y.; Chen, L.; Cao, Q.; Li, Z.; Liu, X. Instability diagnosis and syntrophic acetate oxidation during thermophilic digestion of vegetable waste. *Water Res.* **2018**, *139*, 263–271. [CrossRef]
20. Rodrigues, R.P.; Rodrigues, D.P.; Klepacz-Smolka, A.; Martins, R.C.; Quina, M.J. Comparative analysis of methods and models for predicting biochemical methane potential of various organic substrates. *Sci. Total. Environ.* **2019**, *649*, 1599–1608. [CrossRef]
21. Krapf, L.C.; Heuwinkel, H.; Schmidhalter, U.; Gronauer, A. The potential for online monitoring of short-term process dynamics in anaerobic digestion using near-infrared spectroscopy. *Biomass Bioenergy* **2013**, *48*, 224–230. [CrossRef]
22. Krapf, L.C.; Nast, D.; Gronauer, A.; Schmidhalter, U.; Heuwinkel, H. Transfer of a near infrared spectroscopy laboratory application to an online process analyser for in situ monitoring of anaerobic digestion. *Bioresour. Technol.* **2013**, *129*, 39–50. [CrossRef] [PubMed]
23. Ward, A.J.; Bruni, E.; Lykkegaard, M.K.; Feilberg, A.; Adamsen, A.P.S.; Jensen, A.P.; Poulsen, A.K. Real time monitoring of a biogas digester with gas chromatography, near-infrared spectroscopy, and membrane-inlet mass spectrometry. *Bioresour. Technol.* **2011**, *102*, 4098–4103. [CrossRef]
24. Jacobi, H.F.; Moschner, C.R.; Hartung, E. Use of near infrared spectroscopy in online-monitoring of feeding substrate quality in anaerobic digestion. *Bioresour. Technol.* **2011**, *102*, 4688–4696. [CrossRef] [PubMed]
25. Lesteur, M.; Latrille, E.; Maurel, V.B.; Roger, J.M.; Gonzalez, C.; Junqua, G.; Steyer, J.P. First step towards a fast analytical method for the determination of Biochemical Methane Potential of solid wastes by near infrared spectroscopy. *Bioresour. Technol.* **2011**, *102*, 2280–2288. [CrossRef] [PubMed]
26. Holm-Nielsen, J.B.; Lomberg, C.J.; Oleskowicz-Popiel, P.; Esbensen, K.H. On-line near infrared monitoring of glycerol-boosted anaerobic digestion processes: Evaluation of process analytical technologies. *Biotechnol. Bioeng.* **2008**, *99*, 302–313. [CrossRef]
27. Reed, J.P.; Devlin, D.; Esteves, S.R.R.; Dinsdale, R.; Guwy, A.J. Performance parameter prediction for sewage sludge digesters using reflectance FT-NIR spectroscopy. *Water Res.* **2011**, *45*, 2463–2472. [CrossRef] [PubMed]
28. Saeys, W.; Mouazen, A.M.; Ramon, H. Potential for onsite and online analysis of pig manure using visible and near infrared reflectance spectroscopy. *Biosyst. Eng.* **2005**, *91*, 393–402. [CrossRef]
29. Stockl, A.; Lichti, F. Near-infrared spectroscopy (NIRS) for a real time monitoring of the biogas proces. *Bioresour. Technol.* **2018**, *247*, 1249–1252. [CrossRef]
30. Pearson, K. LIII. On lines and planes of closest fit to systems of points in space. *Lond. Edinb. Dublin Philos. Mag. J. Sci.* **1901**, *2*, 559–572. [CrossRef]
31. Hotelling, H. Analyses of complex statistical variables intro principal components. *J. Educ. Psychol.* **1933**, *24*, 417–441. [CrossRef]
32. Karhunen, K. Uber linear Methoden fur Wahrscheiniogkeitsrechnung. *Ann. Acad. Sci. Fenn. Ser. Al Math. Phys.* **1946**, *37*, 3–79.
33. Loeve, M.M. *Probabilty Theoiry*; Van Nostrand: Princeton, NJ, USA, 1955.
34. Lumley, J.L. *Stochastic Tools in Turbulence*; Academic: New York, NY, USA, 1970.
35. Buljak, V.; Maier, G. Proper Orthogonal Decomposition and Radial Basis Functions in material characterization based on instrumented indentation. *Eng. Struct.* **2011**, *33*, 492–501. [CrossRef]
36. Garbowski, T.; Maier, G.; Novati, G. Novati Diagnosis of concrete dams by flat-jack tests and inverse analyses based on proper orthogonal decomposition. *J. Mech. Mater. Struct.* **2011**, *6*, 181–202. [CrossRef]
37. Garbowski, T.; Maier, G.; Novati, G. Novati On calibration of orthotropic elastic-plastic constitutive models for paper foils by biaxial tests and inverse analyses. *Struct. Multidiscip. Optim.* **2012**, *46*, 111–128. [CrossRef]
38. MacKay, D. Neural networks and machine learning. In *NATO ASI Series, Series F, Computer and Systems Sciences*; Bishop, C.M., Ed.; Kluwer Academic Press: Dordrecht, The Netherlands, 1974–2000; Volume 168, pp. 133–166.
39. Rasmussen, C.E.; Williams, C.K.I. *Gaussian Processes for Machine Learning*; MIT Press: Cambridge, MA, USA, 2006.
40. Sivia, D.; Skilling, J. *Data Analysis: A Bayesian Tutorial*, 2nd ed.; Oxford Science Publications: New York, NY, USA, 2006.
41. Bishop, C.M. *Pattern Recognition and Machine Learning*; Springer: Berlin/Heidelberg, Germany, 2007.
42. Garbowski, T.; Przybyszewski, G. The Sensitivity Analysis of Critical Force in Box Compression Test. *Pol. Pap. Rev.* **2015**, *71*, 275–280. [CrossRef]

43. Alvarez, M.; Lawrence, N. Sparse Convolved Gaussian Processes for Multi-output Regression. In Proceedings of the Twenty-Second Annual Conference on Neural Information Processing Systems (NIPS), Vancouver, BC, Canada, 8–10 December; 2008.
44. Garbowski, T. Stochastic model reduction applied to inverse analysis. In *Adaptive Modeling and Simulation 2013, Proceedings of the VI International Conference on Adaptive Modeling and Simulation ADMOS 2013, Lisbon, Portugal, 3–5 June 2013*; de Almeida, J.P.M., Díez, P., Tiago, C., Parés, N., Eds.; CIMNE: Barcelona, Spain, 2013; pp. 291–300.
45. Mitkowski, P.T.; Adamski, M.; Szaferski, W. Experimental set-up of motionless hydraulic mixer and analysis of hydraulic mixing. *Chem. Eng. J.* **2016**, *288*, 618–637. [CrossRef]
46. Mitkowski, P.T.; Szaferski, W.; Adamski, M. Hydraulic Mixing. In *Practical Aspects of Chemical Engineering, Selected Contributions from PAIC 2017*; Lecture Notes on Multidisciplinary Industrial Engineering; Springer: Cham, Switzerland, 2018; pp. 291–306, ISBN 978-3-319-73978-6. [CrossRef]
47. Czechlowski, M.; Marcinkowski, D.; Berger, W.A.; Golimowski, W. Spectroscopy approach to methanol detection in waste fat methyl esters. *Spectrochim. Acta Part A Mol. Biomol. Spectrosc.* **2019**, *210*, 14–20. [CrossRef]
48. Nespeca, M.G.; Piassalonga, G.B.; de Oliveira, J.E. Infrared spectroscopy and multivariate methods as a tool for identification and quantification of fuels and lubricant oils in soil. *Environ. Monit. Assess.* **2018**, *190*, 72. [CrossRef]
49. Chatterjee, A. An introduction to the proper orthogonal decomposition. *Curr. Sci.* **2000**, *78*, 808–817.
50. Wu, G.G.; Liang, Y.C.; Lin, W.Z.; Lee, H.P.; Lim, S.P. A note on equivalence of proper orthogonal decomposition methods. *J. Sound Vib.* **2003**, *265*, 1103–1110. [CrossRef]
51. Ostrowski, Z.; Białecki, R.A.; Kassab, A.J. Solving inverse heat conduction problems using trained POD-RBF network inverse method. *Inverse Prob. Sci. Eng.* **2008**, *16*, 39–54. [CrossRef]
52. Maier, G.; Bolzon, G.; Buljak, V.; Garbowski, T.; Miller, B. Synergistic combinations of computational methods and experiments for structural diagnosis. In *Computer Methods in Mechanics*; Kuczma, M., Wilmanski, K., Eds.; Lectures of the CMM 2009; Springer: Berlin/Heidelberg, Germany, 2010; pp. 453–476. [CrossRef]
53. Maier, G.; Buljak, V.; Garbowski, T.; Cocchetti, G.; Novati, G. Mechanical characterization of materials and diagnosis of structures by inverse analyses: Some innovative procedures and applications. *Int. J. Comput. Methods* **2014**, *11*, 1343002. [CrossRef]
54. Liang, Y.C.; Lee, H.P.; Lim, S.P.; Lin, W.Z.; Lee, K.H.; Wu, C.G. Proper orthogonal decomposition and its applications—Part I: Theory. *J. Sound Vib.* **2002**, *252*, 527–544. [CrossRef]
55. Nocedal, J.; Wright, S.J. *Numerical Optimization, Springer Series in Operations Research*; Springer: New York, NY, USA, 1999.
56. Insausti, M.; Gomes, A.A.; Cruz, F.V.; Pistonesi, M.F.; Araujo, M.C.U.; Galvão, R.K.H.; Pereira, C.F.; Band, B.S.F. Screening analysis of biodiesel feedstock using UV-vis, NIR and synchronous fluorescence spectrometries and the successive projections algorithm. *Talanta* **2012**, *97*, 579–583. [CrossRef] [PubMed]
57. Shahzad, M.W.; Burhan, M.; Ang, L.; Ng, K.C. Energy-water-environment nexus underpinning future desalination sustainability. *Desalination* **2017**, *413*, 52–64. [CrossRef]